# Biphasic $Ca^{2+}$-Dependent Switching in a Calmodulin−IQ Domain Complex†

D. J. Black, Jared Leonard, and Anthony Persechini*

*Division of Molecular Biology and Biochemistry, University of Missouri, Kansas City, Missouri 64110-2499*

*Received December 12, 2005; Revised Manuscript Received February 23, 2006*

ABSTRACT: The relationship between the free $Ca^{2+}$ concentration and the apparent dissociation constant for the complex between calmodulin (CaM) and the neuromodulin IQ domain consists of two phases. In the first phase, $Ca^{2+}$ bound to the C-ter EF hand pair in CaM increases the $K_d$ for the complex from the $Ca^{2+}$-free value of 2.3 ± 0.1 $\mu$M to a value of 14.4 ± 1.3 $\mu$M. In the second phase, $Ca^{2+}$ bound to the N-ter EF hand pair reduces the $K_d$ for the complex to a value of 2.5 ± 0.1 $\mu$M, reversing the effect of the first phase. Due to energy coupling effects associated with these phases, the mean dissociation constant for binding of $Ca^{2+}$ to the C-ter EF hand pair is increased ∼3-fold, from 1.8 ± 0.1 to 5.1 ± 0.7 $\mu$M, and the mean dissociation constant for binding of $Ca^{2+}$ to the N-ter EF hand pair is decreased by the same factor, from 11.2 ± 1.0 to 3.5 ± 0.6 $\mu$M. These characteristics produce a bell-shaped relationship between the apparent dissociation constant for the complex and the free $Ca^{2+}$ concentration, with a distance of 5−6 $\mu$M between the midpoints of the rising and falling phases. Release of CaM from the neuromodulin IQ domain therefore appears to be promoted over a relatively narrow range of free $Ca^{2+}$ concentrations. Our results demonstrate that CaM−IQ domain complexes can function as biphasic $Ca^{2+}$ switches through opposing effects of $Ca^{2+}$ bound sequentially to the two EF hand pairs in CaM.

The $Ca^{2+}$-binding protein calmodulin (CaM)[1] plays a central role in transducing $Ca^{2+}$ signals through its interactions with more than 30 different target proteins. Many of these, such as phosphodiesterase, myosin light chain kinase, and the constitutive nitric oxide synthases, do not interact significantly with $Ca^{2+}$-free CaM (apoCaM) (*1*−*4*). However, a large class of targets bind apoCaM at least as well as the $Ca^{2+}$-liganded forms of the protein. The majority of these, including neuromodulin, neurogranin, the unconventional myosins and some $Ca^{2+}$, $K^+$, and $Na^+$ channels, interact with CaM via IQ domains, which have the consensus sequence [I,L,V]QxxxR[G,x]xxx[R,K] (*5*, *6*). These regions bind apoCaM and/or $Ca^{2+}$-liganded CaM with dissociation constants ranging from sub-nanomolar to micromolar, depending upon their precise sequence and context (*6*). CaM−IQ domain complexes have been implicated in a variety of regulatory processes, including positive and negative regulation of ion channels and unconventional myosin-based motility (*6*). Some IQ domain proteins have been proposed to function as local intracellular stores of CaM (*7*).

The potential importance of such stores has been heightened by recent investigations indicating that the intracellular CaM concentration is limiting. We have found that a dephosphorylation-dependent increase in the amount of CaM bound to nitric oxide synthase in endothelial cells significantly reduces the available CaM concentration during a $Ca^{2+}$ signal and inhibits the activity of the plasma membrane $Ca^{2+}$ pump and presumably other CaM targets (*8*). Rahkilin and co-workers have recently demonstrated that a limiting CaM concentration in neurons results in similar coupling among target activities (*9*). Finally, the work of Isotani and co-workers suggests that the CaM concentration is limiting in smooth muscle tissue (*10*). Thus, CaM and its targets can be considered to form what we have termed the CaM network (*11*). Although the available CaM concentration is a function of all its various interactions, proteins that function as CaM stores are of particular interest, as they are likely to contribute in important ways to the form and function of the CaM network. Neuromodulin, a neuronal IQ domain protein found in axons and terminals, is perhaps the best studied example of such a protein (*7*). Neurogranin, a smaller protein with an essentially identical IQ domain, is thought to perform a similar function in dendritic spines (*12*, *13*).

In this paper, we describe a steady-state mechanism for $Ca^{2+}$-dependent switching in the neuromodulin CaM−IQ domain complex. A surprising aspect of this mechanism is its fundamentally biphasic nature: $Ca^{2+}$ binding one EF hand pair in CaM decreases the affinity of the complex, and binding to the other then completely reverses this effect. The

† This work was supported by NIH Grant GM074887 to A.P.

* To whom correspondence should be addressed: Division of Molecular Biology and Biochemistry, University of Missouri, 5007 Rockhill Rd., Kansas City, MO 64110-2499. Telephone: (816) 235-6076. Fax: (816) 235-5595. E-mail: Persechinia@umkc.edu.

[1] Abbreviations: $BSCaM_{IQ}$, fluorescent biosensor containing a CaM-binding sequence based on the IQ domain in neuromodulin; CaM, calmodulin; ECFP, cyan-emitting variant of green fluorescent protein; $EYFP_C$, yellow-emitting variant of green fluorescent protein that has been modified to reduce the dependence of its fluorescence emission on pH over the physiological pH range; $N_xCCaM$ ($N_xC$), mutant CaM with E31A and E67A substitutions; $NC_xCaM$ ($NC_x$), mutant CaM with E104A and E140A substitutions; $N_2CCaM$ ($N_2C$), CaM with $Ca^{2+}$ bound to both N-ter EF hands; $NC_2CaM$ ($NC_2$), CaM with $Ca^{2+}$ bound to both C-ter EF hands; $N_2C_2CaM$ ($N_2C_2$), CaM with $Ca^{2+}$ bound to all four EF hands; $N_2C_xCaM$ ($N_2C_x$) and $N_xC_2CaM$ ($N_xC_2$), mutant CaMs with $Ca^{2+}$ bound to the remaining functional EF hands; $K_{1,2}$, geometric mean of $K_1$ and $K_2$; $K_{3,4}$, geometric mean of $K_3$ and $K_4$; BAPTA, 1,2-bis(2-aminophenoxy)ethane-*N*,*N*,*N*′,*N*′-tetraacetic acid; dibromo-BAPTA, 1,2-bis(2-amino-5,5′-dibromophenoxy)ethane-*N*,*N*,*N*′,*N*′-tetraacetic acid; FRET, fluorescence resonance energy transfer.

10.1021/bi052533w CCC: $33.50 
Published on Web 05/10/2006

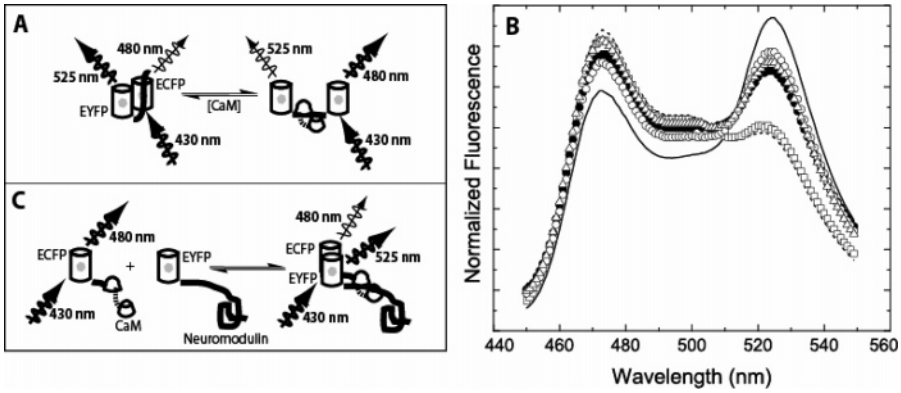


FIGURE 1: Fluorescent reporter systems used to monitor interactions between CaM and the neuromodulin IQ domain. (A) $BSCaM_{IQ}$ consists of ECFP and EYFP variants of GFP joined by an IQ domain. When CaM is bound to this domain, changes in the orientation and/or distance between the two fluorescent proteins decrease the extent of fluorescence resonance energy transfer (FRET) between the ECFP and EYFP components. Thus, under 430 nm excitation, ECFP donor fluorescence, measured at 480 nm, is increased and EYFP acceptor fluorescence, measured at 525 nm, is decreased. (B) Complete fluorescence emission spectra for $BSCaM_{IQ}$ under 430 nm excitation. The solid line is the emission spectrum determined in the absence of CaM, and the dashed line is the spectrum determined in the presence of a saturating apoCaM concentration. The remaining spectra were determined in the presence of saturating concentrations of $Ca^{2+}$-free $NC_xCaM$ or $N_xCCaM$ (□), $Ca^{2+}$-saturated native CaM (●), $N_xC_2CaM$ (○), and $N_2C_xCaM$ (△). (C) A bipartite reporter system consisting of ECFP−CaM and EYFP−neuromodulin fusion proteins. As illustrated in the figure, formation of the complex between CaM and neuromodulin allows FRET between the ECFP and EYFP labels to occur under 430 nm excitation.

result is a bell-shaped relationship between the apparent dissociation constant for the complex and the free $Ca^{2+}$ concentration.

## MATERIALS AND METHODS

*Proteins.* The cDNA encoding $BSCaM_{IQ}$, a fluorescent reporter that binds CaM via an IQ domain sequence derived from neuromodulin, was assembled in a modified pET30a vector (Novagen, Inc.). The composition of $BSCaM_{IQ}$ is similar to that of other CaM biosensors we have developed (*14*, *15*), except that it contains a form of enhanced yellow fluorescent protein ($EYFP_C$) in which the $pK_a$ for fluorescence quenching is shifted from ~7 to ~6, which increases EYFP fluorescence emission under the conditions used in these investigations (*16*). The CaM-binding sequence bridging the ECFP and $EYFP_C$ variants in $BSCaM_{IQ}$, AAATKIQA[A]FRGHITRKKLKGEKKGAA, is based on the IQ domain region in neuromodulin (neuromodulin sequence underlined), differing only in the substitution of an Ala residue (in brackets) for a Ser. This corresponds with position 41 in the neuromodulin amino acid sequence (*17*). Phosphorylation at this position in full-length neuromodulin blocks CaM binding, but substitution of a Gly residue does not affect binding (*17*). We have also developed a bipartite fluorescent reporter system consisting of $EYFP_C$−neuromodulin and ECFP−CaM fusion proteins. In the neuromodulin fusion, the fluorescent protein is joined to the N-terminus of full-length native neuromodulin via a Gly-Thr amino acid pair. In the CaM fusion, the fluorescent protein is joined to the N-terminus of native CaM via a GASGSAAAG polypeptide linker. All fluorescent protein constructs were expressed with amino-terminal six-His tags in BL21(DE3) and were purified using $Ni^+$-chelate affinity chromatography as described previously (*18*). Both of these fluorescent reporter systems are represented schematically in Figure 1.

Native and mutant CaMs were expressed and purified as described in detail elsewhere (*19*, *20*). The two mutant CaMs used in these studies are $N_xCCaM$ ($N_xC$), in which glutamic acid residues at positions 31 and 67 in the N-ter EF hands have been replaced with alanines, and $NC_xCaM$ ($NC_x$), in which the homologous glutamic acid residues at positions 104 and 140 have been replaced. These mutations eliminate binding of $Ca^{2+}$ to the N-ter or C-ter EF hand pair, as indicated by the subscript *x*.

*Fluorescence Measurements.* A Photon Technologies International (Monmouth Junction, NJ) QM-1 fluorometer operated in photon-counting mode was used for all steady-state fluorescence measurements. Monochromator excitation and emission slit widths were set to produce bandwidths of ~2.5 nm. All experiments were performed at 23 °C. The standard experimental buffer contained 25 mM Tris (pH 7.5), 0.1 M KCl, 100 μg/mL BSA, and other components as specified in the text or captions. For analysis of the $Ca^{2+}$ dependencies of native and mutant CaM complexes, buffered free $Ca^{2+}$ concentrations were produced using 1.5 mM BAPTA, 1.5 mM dibromo-BAPTA, and various amounts of added $CaCl_2$. Stated free $Ca^{2+}$ concentrations were measured using 250 nM indo-5F or mag indo-1 according to established procedures (Invitrogen, Inc.). As we have demonstrated elsewhere, there is no significant spillover in the fluorescence emissions of these $Ca^{2+}$ indicator dyes and the $BSCaM_{IQ}$ reporter (*8*, *21*).

When required, proteins and buffers were decalcified by successive treatments with Chelex and a BAPTA-polystyrene column (Invitrogen, Inc.). Contaminating amounts of $Ca^{2+}$ in protein solutions at their stated working concentrations were ≤150 nM, based on the absence of any detectable effect on the $A_{263}$ of dibromo-BAPTA.

*Analysis of Fluorescence Data.* Fractional changes in fluorescence were analyzed to extract apparent $K_d$ values for native or mutant CaMs using a standard hyperbolic binding equation, where FR is fractional response as defined in the relevant figure legends:

$$FR = [CaM]/([CaM] + K_d) \quad (1)$$

A sequential $Ca^{2+}$ binding model was used to analyze fractional changes in fluorescence due to $Ca^{2+}$-dependent

Table 1: Apparent $K_d$ Values for the Complexes between $BSCaM_{IQ}$ and Native or Mutant CaMs[a]

| | NC−B | $N_2C_2$−B | $NC_x$−B | $N_2C_x$−B | $N_xC$−B | $N_xC_2$−B | $NC_2$−B |
|---|---|---|---|---|---|---|---|
| $K_d$ ($\mu$M) | 2.3 ± 0.1 | 2.5 ± 0.1 | 2.5 ± 0.3 | 36.7 ± 3.9 | 2.1 ± 0.2 | 14.4 ± 1.3 | 10.8 ± 1.1 |
| $F_{min}/F_{max}$ | 0.68 ± 0.2 | 0.83 ± 0.3 | 0.69 ± 0.2 | 0.83 ± 0.3 | 0.68 ± 0.2 | 0.85 ± 0.2 | 0.85 ± 0.2 |

[a] B refers to bound $BSCaM_{IQ}$. N and C refer to the C-ter and N-ter EF hand pairs in CaM, respectively, with subscripts indicating the $Ca^{2+}$-liganded state or the inability to bind $Ca^{2+}$ due to mutagenesis ($x$). The absence of a subscript indicates a native $Ca^{2+}$-free EF hand pair. The nominal affinity given for the $NC_2$−B complex was determined at a free $Ca^{2+}$ concentration of 10 $\mu$M. Standard errors were derived from the diagonal elements in the variance−covariance matrices for the fitted curves. $F_{min}/F_{max}$ is the ratio of the 525 nm fluorescence emissions of the $BSCaM_{IQ}$ complex with native or mutant CaM ($F_{min}$) to the emission of free $BSCaM_{IQ}$ ($F_{max}$).

Table 2: $Ca^{2+}$ Binding Constants for Native and Mutant CaMs in the Presence and Absence of $BSCaM_{IQ}$[a]

| | $K_1$ ($\mu$M) | $K_2$ ($\mu$M) | $K_3$ ($\mu$M) | $K_4$ ($\mu$M) | $K_{1,2}$ ($\mu$M) | $K_{3,4}$ ($\mu$M) | $K_1K_2$ ($\mu M^2$) | $K_3K_4$ ($\mu M^2$) |
|---|---|---|---|---|---|---|---|---|
| NC | 11.2 ± 5.4 | 0.3 ± 0.2 | 25.1 ± 10.3 | 5.0 ± 2.6 | 1.8 ± 0.1 | 11.2 ± 1.0 | 3.1 ± 0.2 | 126 ± 11.4 |
| $N_xC$ | 14.1 ± 4.9 | 0.2 ± 0.1 | − | − | 1.6 ± 0.2 | − | 2.4 ± 0.3 | − |
| $NC_x$ | − | − | 24.0 ± 9.5 | 3.9 ± 1.6 | − | 9.7 ± 1.0 | − | 93.3 ± 9.2 |
| NC−B | 10.7 ± 3.8 | 2.4 ± 0.8 | 7.8 ± 3 | 1.6 ± 0.7 | 5.1 ± 0.7 | 3.5 ± 0.6 | 25.7 ± 3.5 | 12.3 ± 1.9 |
| $N_xC$−B | 22.4 ± 11.3 | 1.1 ± 0.6 | − | − | 4.9 ± 0.5 | − | 24.6 ± 2.7 | − |
| $N_xC$−$B^F$ | 23.2 ± 8.6 | 0.7 ± 0.2 | − | − | 4.0 ± 0.3 | − | 16.1 ± 1.1 | − |
| $NC_x$−$B^F$ | − | − | 122 ± 68.0 | 9.4 ± 4.0 | − | 33.8 ± 4.0 | − | 1140 ± 122.0 |

[a] The nomenclature used here is defined in the footnote of Table 1. The superscript F identifies dissociation constants derived from data for $Ca^{2+}$-dependent dissociation of mutant CaM−$BSCaM_{IQ}$ complexes. Otherwise, all dissociation constants were derived from direct $Ca^{2+}$ binding measurements as described in Materials and Methods. Standard errors were derived from the diagonal elements in the variance−covariance matrices for fits to at least five pooled data sets. $K_{1,2}$ and $K_{3,4}$ are the geometric means of the $Ca^{2+}$ binding constants for the C-ter and N-ter EF hand pairs, respectively.

dissociation of the $N_x$CCaM or $NC_x$CaM complexes with $BSCaM_{IQ}$:

$$FR = \frac{([Ca^{2+}]^2/K_1K_2)}{(1 + [Ca^{2+}]/K_1 + [Ca^{2+}]^2/K_1K_2)} \quad (2)$$

where $K_1$ and $K_2$ in this case designate the apparent dissociation constants for the two sites in the functional EF hand pairs. A sequential mechanism for binding of $Ca^{2+}$ to the individual EF hands is assumed. This is supported by investigations in which binding of $Ca^{2+}$ to individual EF hands have been monitored spectrally (*22*−*24*). We have also assumed that dissociation requires occupancy of both sites in an EF hand pair. This may not be strictly correct, since NMR investigations indicate that occupancy of a single $Ca^{2+}$-binding site can produce significant conformational changes in CaM (*24*). However, under steady-state conditions, positive cooperativity between the sites in each EF hand pair restricts the amount of CaM with only one site occupied to negligible levels (*25*).

*Direct Determinations of $Ca^{2+}$ Binding Constants.* Direct $Ca^{2+}$ binding measurements were performed as described by Linse and co-workers (*26*, *27*). In this approach, binding of $Ca^{2+}$ to a BAPTA or dibromo-BAPTA chelator is measured on the basis of its optical absorbance at 263 nm as known increments of $Ca^{2+}$ are added to an initially decalcified solution containing the chelator and the $Ca^{2+}$-binding protein of interest. The absolute amounts of free $Ca^{2+}$ and $Ca^{2+}$ bound to the chelator after each addition can thus be estimated, with the amount bound to the protein accounting for the remainder (*28*). We have found a 0.5:1 molar ratio of chelator to protein $Ca^{2+}$ binding sites to yield the best determined $Ca^{2+}$ dissociation constants. Apparent $Ca^{2+}$ dissociation constants for proteins were derived from direct fits to observed chelator absorbance using the *Caligator* software package (*28*). A general four-site Adair equation was used to define binding of $Ca^{2+}$ to native CaM:

$$\theta = {}^1/_4[(K_1[Ca^{2+}] + 2K_1K_2[Ca^{2+}]^2 + 3K_1K_2K_3[Ca^{2+}]^3 + 4K_1K_2K_3K_4[Ca^{2+}]^4)/(1 + K_1[Ca^{2+}] + K_1K_2[Ca^{2+}]^2 + K_1K_2K_3[Ca^{2+}]^3 + K_1K_2K_3K_4[Ca^{2+}]^4)] \quad (3)$$

where $\theta$ is the fractional saturation of the four sites in this protein. An abbreviated form of this expression was used to describe binding to the two CaM mutants, $NC_x$CaM and $N_x$CCaM, which have only one functional EF hand pair:

$$\theta = {}^1/_2[(K_1[Ca^{2+}] + 2K_1K_2[Ca^{2+}]^2)/(1 + K_1[Ca^{2+}] + K_1K_2[Ca^{2+}]^2)] \quad (4)$$

*Modeling.* The theoretical curves presented in Figures 8 and 9 were calculated using the *Berkeley Madonna* software package (Macey and Oster, Inc.). For this purpose, an expanded version of the scheme presented in Figure 7 was used in which binding of $Ca^{2+}$ to each EF hand pair is treated as a two-step sequential process. Since all simulations were allowed to reach a steady state, only the ratios of the rate constants used for each step in the mechanism are important, and these are defined by the steady-state interaction parameters listed in Tables 1 and 2.

## RESULTS

*Binding of Native and Mutant CaMs to $BSCaM_{IQ}$ in the Presence and Absence of $Ca^{2+}$.* The initial step in these investigations was to determine $K_d$ values for the complexes between the $BSCaM_{IQ}$ fluorescent reporter containing the neuromodulin IQ domain and apoCaM or $(Ca^{2+})_4$-CaM. Values of 2.3 ± 0.1 and 2.5 ± 0.1 $\mu$M, respectively, were derived from the data presented in Figure 2 (Table 1). Purified neuromodulin has previously been reported to bind apoCaM and $(Ca^{2+})_4$-CaM with $K_d$ values of 3.0 and 3.4 $\mu$M, respectively, under similar experimental conditions (*29*,

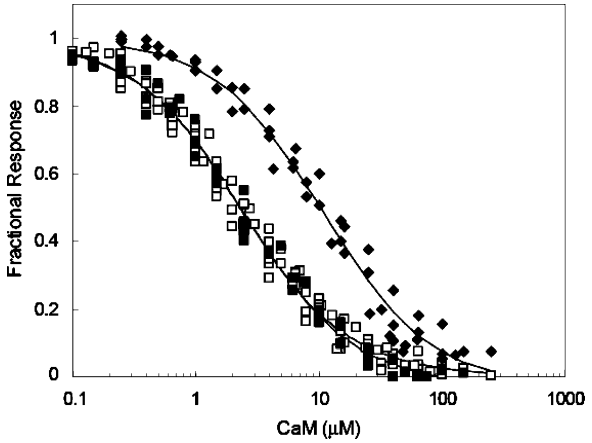


FIGURE 2: Binding of CaM to $BSCaM_{IQ}$ in the presence of 10 (◆) and 250 $\mu$M free $Ca^{2+}$ (□) or 3 mM BAPTA (■). The fractional change in 525 nm fluorescence produced by the decrease in the extent of FRET associated with formation of the complex is defined as $(F_{max} - F)/(F_{max} - F_{min})$, where $F$ corresponds to the emission measured after each addition and $F_{max}$ and $F_{min}$ correspond to the emissions of CaM-free and CaM-saturated $BSCaM_{IQ}$, respectively. A 50 $\mu$M $BSCaM_{IQ}$ concentration was used for these experiments. The apparent $K_d$ values determined from fits of these data to a simple one-site hyperbolic binding equation (not shown) are listed in Table 1.

*30*). As seen in Figure 2, at a free $Ca^{2+}$ concentration of 10 $\mu$M, the apparent $K_d$ value for the CaM−$BSCaM_{IQ}$ complex increases to 10.8 ± 1.1 $\mu$M, suggesting that the transition between the apoCaM and $(Ca^{2+})_4$-CaM complexes involves more weakly bound forms of CaM (Table 1).

To further investigate the basis for this apparent reduction in affinity at an intermediate free $Ca^{2+}$ concentration, we employed $N_x$CCaM and $NC_x$CaM, mutants of CaM in which binding of $Ca^{2+}$ to the N-ter or C-ter EF hand pair has been abolished (*19*). These mutants provide a convenient way of isolating the effects of binding of $Ca^{2+}$ to each EF hand pair. Our results indicate that the properties of these mutant proteins are consistent with the properties of native CaM. Nevertheless, it should be borne in mind that the mutant EF hands in these proteins are likely to adopt conformations that differ from the corresponding native $Ca^{2+}$-free conformations (*31*). As seen in Figure 3A, in the absence of $Ca^{2+}$, both mutants bind the $BSCaM_{IQ}$ reporter with a $K_d$ value of ~2.3 $\mu$M, essentially identical to the value for native apoCaM (Table 1). In the presence of a saturating $Ca^{2+}$ concentration, the $K_d$ values for the complexes with $N_x$CCaM and $NC_x$CaM are increased to 14.4 ± 1.3 and 36.7 ± 3.9 $\mu$M, respectively (Figure 3B and Table 1). Data for dissociation of the mutant CaM complexes as a function of the free $Ca^{2+}$ concentration are presented in Figure 4. Binding constants for the functional EF hand pair in each mutant complex can be estimated on the basis of fits of these data to eq 2 (Table 2). The geometric means of the dissociation constants derived for the C-ter ($K_{1,2}$) and N-ter ($K_{3,4}$) EF hand pairs in bound $N_x$CCaM and $NC_x$CaM are 4.0 ± 0.3 and 33.8 ± 4.0 $\mu$M, respectively; the corresponding values for the free mutant proteins are 1.6 ± 0.2 and 9.7 ± 1.0, respectively (Table 2). Thus, the mean $Ca^{2+}$ binding affinities of the functional EF hand pairs in both mutant CaMs are reduced 3−4-fold when they are associated with $BSCaM_{IQ}$.

*$Ca^{2+}$ Binding to Native and Mutant CaMs in the Presence and Absence of $BSCaM_{IQ}$.* $Ca^{2+}$ binding data measured in the presence and absence of $BSCaM_{IQ}$ are presented in panels A and B of Figure 5. Significant dissociation of CaM from the IQ domain is prevented during the course of these experiments by using at total concentration of CaM and $BSCaM_{IQ}$ that is ~10-fold or more above the $K_d$ value for the lowest-affinity form of the complex. Otherwise, one observes the $Ca^{2+}$ binding characteristics of a mixture of free and bound CaM. Indeeed, this technique could not be applied to the complex of $NC_x$CaM and $BSCaM_{IQ}$ because a total protein concentration of ~200 $\mu$M is required to prevent dissociation of this complex at elevated free $Ca^{2+}$ concentrations, which was found to be above the usable limit due to solubility problems.

The $Ca^{2+}$ binding constants we have derived for native CaM are essentially identical to the literature values (*27*), and the correspondence between these values and those determined for the $N_x$CCaM and $NC_x$CaM mutants suggests that the presence of a nonfunctional EF hand pair in one

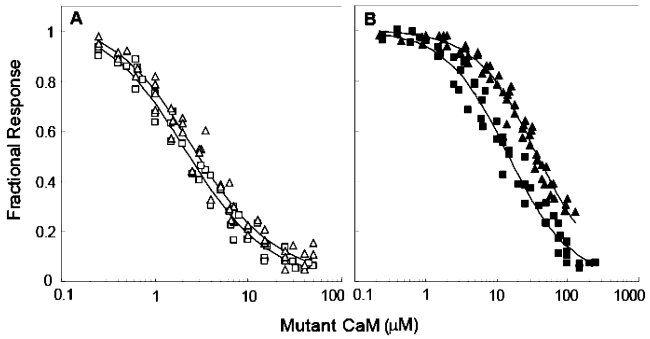


FIGURE 3: Binding of $N_x$CCaM or $NC_x$CaM to $BSCaM_{IQ}$. (A) Fractional changes in 525 nm fluorescence emission, defined as described in the legend of Figure 2, associated with binding of $N_x$CCaM (□) or $NC_x$CaM (△) to 50 nM $BSCaM_{IQ}$ under nominally $Ca^{2+}$-free conditions (3 mM BAPTA). (B) Fractional changes in 525 nm fluorescence emission associated with binding of $N_x$CCaM (■) and $NC_x$CaM (▲) to 150 nM $BSCaM_{IQ}$ at a free $Ca^{2+}$ concentration of ~250 $\mu$M. Apparent $K_d$ values derived from the data presented in panels A and B are listed in Table 1.

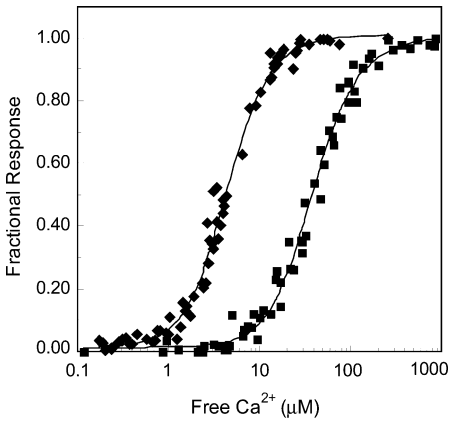


FIGURE 4: $Ca^{2+}$-dependent dissociation of the $N_x$CCaM or $NC_x$-CaM complexes with $BSCaM_{IQ}$. Fractional changes in 525 nm fluorescence emission associated with formation of the complexes between 12.5 $\mu$M $BSCaM_{IQ}$ and 1 $\mu$M $N_x$CCaM (◆) or $NC_x$CaM (■). All free $Ca^{2+}$ concentrations were verified using indo-5F or mag-indo-1. Fractional changes in fluorescence are defined using an $F_{max}$ value measured at the end of the experiment, which accounts for residual CaM binding in the presence of $Ca^{2+}$. Otherwise, fractional changes are defined as described in the legend of Figure 2. Apparent $Ca^{2+}$ binding constants derived from fits of these data to eq 2 are listed in Table 2.

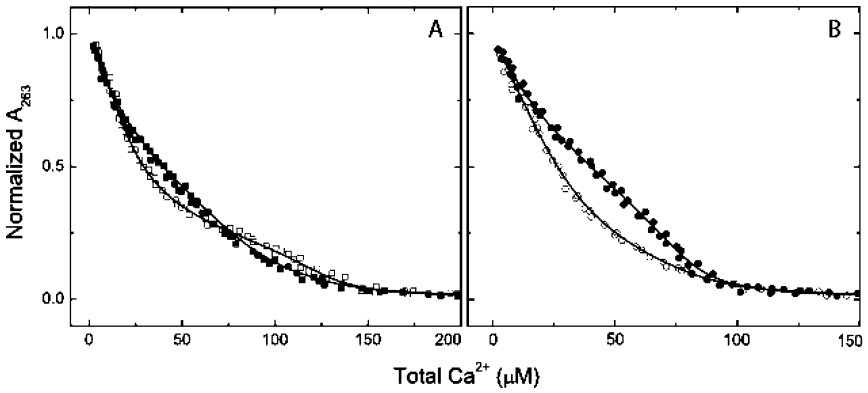


FIGURE 5: Direct measurements of the degree of binding of $Ca^{2+}$ to native and mutant CaMs in the presence and absence of $BSCaM_{IQ}$. (A) Absorbance data (263 nm) for 40 $\mu$M dibromo-BAPTA measured in the presence of 20 $\mu$M native CaM (■) or 20 $\mu$M native CaM and 100 $\mu$M $BSCaM_{IQ}$ (□). (B) Absorbance data for 40 $\mu$M dibromo-BAPTA measured in the presence of 20 $\mu$M $N_xCCaM$ (●) or 20 $\mu$M $N_xCCaM$ and 100 $\mu$M $BSCaM_{IQ}$ (○). For presentation purposes, these data have been normalized to the absorbance of $Ca^{2+}$-free dibromo-BAPTA determimed at the completion of each titration experiment. Pooled data from three separate $Ca^{2+}$ binding experiments are presented for each set of conditions. The dissociation constants derived from fits of these and similar data to eq 3 or 4 are listed in Table 2 (*28*).

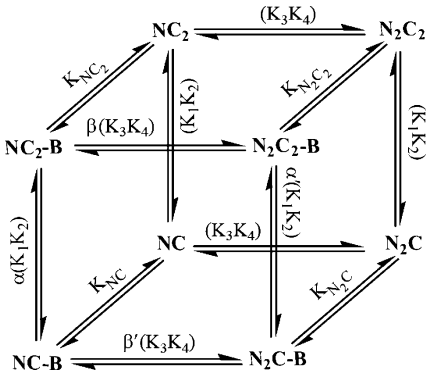


FIGURE 6: General four-state scheme for $Ca^{2+}$-dependent switching in a CaM−IQ domain complex. B indicates the bound IQ domain protein; N and C indicate the N-ter and C-ter EF hand pairs in CaM, respectively, with subscripts denoting their $Ca^{2+}$-liganded states. The absence of a subscript indicates a $Ca^{2+}$-free EF hand pair.

CaM lobe does not significantly perturb binding of $Ca^{2+}$ to the other (Table 2). There is also reasonable agreement between the mean dissociation constants for the C-ter EF hand pair ($K_{1,2}$) derived for the $N_xCCaM-BSCaM_{IQ}$ complex based on data for $Ca^{2+}$-dependent dissociation (4.0 ± 0.3) and from direct measurements of $Ca^{2+}$ binding (4.9 ± 0.5). Perhaps most importantly, our results demonstrate that in the native $CaM-BSCaM_{IQ}$ complex the affinity of the C-ter EF hand pair in CaM is decreased and the affinity of the N-ter EF hand pair is increased. These opposing effects result in similar mean dissociation constants of 5.1 ± 0.7 and 3.5 ± 0.6 $\mu$M for the two EF hand pairs. The first of these values is assumed to be $K_{1,2}$, the mean dissociation constant for the C-ter EF hand pair, because it is closest to the value for the $N_xCCaM-BSCaM_{IQ}$ complex (Table 2).

*A General Four-State Mechanism for $Ca^{2+}$-Dependent Switching in a CaM−Target Complex.* A general steady-state mechanism for $Ca^{2+}$-dependent switching in a CaM−IQ domain complex is presented in Figure 6. It includes the four major $Ca^{2+}$-liganded forms of CaM: apoCaM (NC), CaM with two $Ca^{2+}$ ions bound to the C-ter ($NC_2$) or N-ter ($N_2C$) EF hand pair, and CaM with $Ca^{2+}$ bound to both EF hand pairs ($N_2C_2$). In this model, binding of $Ca^{2+}$ to the individual sites in an EF hand pair is treated as a single step governed by a $K_1K_2$ or $K_3K_4$ value.

*Thermodynamic Relationships.* Thermodynamic linkage or energy coupling associated with formation of a CaM−target complex can be quantitively defined according to the relation

$$\Delta\Delta G_C = RT \ln \frac{K_{N_2C_2}}{K_{NC}} = RT \ln \frac{(K_1K_2K_3K_4)_B}{(K_1K_2K_3K_4)_F} \quad (5)$$

where $K_1$ and $K_2$ are the $Ca^{2+}$ binding constants for the C-ter EF hand pair and $K_3$ and $K_4$ are the constants for the N-ter pair. $K_{NC}$ and $K_{N_2C_2}$ are the dissociation constants for the apoCaM (NC) and $(Ca^{2+})_4$-CaM ($N_2C_2$) complexes with a target, respectively. The subscripts F and B identify the $Ca^{2+}$ binding constants for free CaM and CaM bound to a target, respectively. These mathematical relationships formalize the basic thermodynamic requirement that a $Ca^{2+}$-dependent change in the affinity of a CaM−target complex must be coupled to a corresponding change in the $Ca^{2+}$ binding affinity of CaM when it is bound to the target. A negative $\Delta\Delta G_C$ value is produced when $Ca^{2+}$ binding increases the affinity of CaM for a target. This is termed favorable or "positive" energy coupling because it is linked to an increase in $Ca^{2+}$ binding affinity. A positive $\Delta\Delta G_C$ value is produced when $Ca^{2+}$ binding decreases the affinity of CaM for a target. This type of energy coupling is termed unfavorable or "negative" because it is linked to a decrease in $Ca^{2+}$ binding affinity. We can also define energy coupling in terms of the individual EF hand pairs:

$$\Delta\Delta G_C^C = RT \ln \alpha, \text{ where } \alpha = \frac{K_{NC_2}}{K_{NC}} = \frac{(K_1K_2)_B}{(K_1K_2)_F} \quad (6)$$

$$\Delta\Delta G_C^N = RT \ln \beta, \text{ where } \beta = \frac{K_{N_2C_2}}{K_{NC_2}} = \frac{(K_3K_4)_B}{(K_3K_4)_F} \quad (7)$$

The superscripts C and N designate the $\Delta\Delta G_C$ values for the C-ter and N-ter EF hand pairs, respectively. The proportionality constants $\alpha$ and $\beta$ are coupling coefficients; values of $<1$ correspond with positive coupling, and values of $>1$ correspond with negative coupling. As seen in Figure 6, $Ca^{2+}$ can in principle bind first to either the N-ter or C-ter EF hand pair, so two sets of coupling coefficients and $\Delta\Delta G$ values must be considered. Unprimed symbols are used for

Table 3: Coupling Coefficients and $\Delta\Delta G_C$ Values for the CaM−BSCaM$_{IQ}$ Complex[a]

| | $K_{N_xC_2}/K_{N_xC}$ | $(K_1K_2)_{N_xC-B}/(K_1K_2)_{N_xC}$ | $(K_1K_2)_{NC-B}/(K_1K_2)_{NC}$ |
|---|---|---|---|
| $\alpha$ | $6.9 \pm 0.9$ | $10.3 \pm 1.7$ | $8.3 \pm 1.2$ |
| $\Delta\Delta G_C^C$ | $1.14 \pm 0.08$ | $1.4 \pm 0.1$ | $1.25 \pm 0.1$ |
| | | | $K_{N_2C_2}/K_{N_2C_x}$ |
| $\alpha'$ | | | $0.07 \pm 0.01$ |
| $\Delta\Delta G_C^{C'}$ | | | $-1.59 \pm 0.07$ |
| | $K_{N_2C_2}/K_{N_xC_2}$ | | $(K_3K_4)_{NC_2-B}/(K_3K_4)_{NC_2}$ |
| $\beta$ | $0.17 \pm 0.02$ | | $0.1 \pm 0.02$ |
| $\Delta\Delta G_C^N$ | $-1.03 \pm 0.06$ | | $-1.4 \pm 0.1$ |
| | $K_{N_2C_x}/K_{NC_x}$ | | $(K_3K_4)^F_{NC_x-B}/(K_3K_4)_{NC_x}$ |
| $\beta'$ | $14.7 \pm 2.4$ | | $12.2 \pm 1.8$ |
| $\Delta\Delta G_C^{N'}$ | $1.58 \pm 0.1$ | | $1.48 \pm 0.1$ |

[a] The $K_3K_4$ value indicated with a superscript F was derived from data for $Ca^{2+}$-dependent dissociation of the $NC_x$−B complex. All other $K_1K_2$ and $K_3K_4$ values were derived from direct measurements of $Ca^{2+}$ binding. Dissociation constants for the various CaM−BSCaM$_{IQ}$ complexes are designated by subscripts identifying the bound CaM species. The products of the dissociation constants for the EF hand pairs are designated by subscripts identifying the bound or free CaM species. The nomenclature used for these subscripts is defined in the footnotes of Tables 1 and 2. Values given for $\Delta\Delta G_C$ and coupling coefficients were calculated according to eqs 6 and 7. As depicted in Figure 6, unprimed values are those for the favored C-ter → N-ter order of $Ca^{2+}$ binding, and primed values are those for the alternative N-ter → C-ter order of binding.

the C-ter → N-ter pathway and primed symbols for the alternative N-ter → C-ter pathway (see Figure 6). Since the apoCaM and $(Ca^{2+})_4$-CaM complexes with BSCaM$_{IQ}$ have essentially identical affinities, the complete transition from one type of complex to the other cannot produce significant net energy coupling ($\Delta\Delta G_C \approx 0$). In terms of the individual EF hand pairs, this means that $\Delta\Delta G_C^C + \Delta\Delta G_C^N \approx \Delta\Delta G_C^{C'} + \Delta\Delta G_C^{N'} \approx 0$ and $\alpha\beta \approx \alpha'\beta' \approx 1$. Thus, despite an overall lack of energy coupling, energetically opposing effects of binding of $Ca^{2+}$ to the two EF hand pairs are not precluded, and this is in fact what we have observed.

As seen in Table 3, $\alpha$ has a value of ~8.5, indicating negative coupling, while $\beta$ has a value of ~0.14, indicating positive coupling. The product of these values is ~1.2, satisfying the requirement that $\alpha\beta \approx 1$. Thus, along the C-ter → N-ter pathway, negatively coupled binding of $Ca^{2+}$ to the C-ter EF hand pair, which necessarily reduces the affinity of the CaM−BSCaM$_{IQ}$ complex, is followed by positively coupled binding to the N-ter EF hand, which in this case necessarily restores the affinity of the complex to its initial value. On the basis of the properties of the $NC_x$CaM−BSCaM$_{IQ}$ complex, we have estimated a value of ~13.5 for $\beta'$, the coupling coefficient for the first step in the alternative N-ter → C-ter pathway (Table 3). This pathway thus appears to be strongly disfavored for at least three reasons. (1) The $Ca^{2+}$ binding affinity of the N-ter EF hand pair in CaM is inherently ~6-fold lower than the affinity of the C-ter pair (Table 2). (2) The $\beta'$ value is ~2-fold larger than the $\alpha$ value, which widens this inherent difference by ~30%. (3) The affinity of the $N_2$CCaM complex with BSCaM$_{IQ}$ is 2-fold lower than the affinity of the $NC_2$CaM complex (Table 1). Thus, we can simplify our steady-state scheme by omitting the N-ter → C-ter pathway (Figure 7). This pathway is likely to be more important under transient conditions because the N-ter EF hand pair binds $Ca^{2+}$ more rapidly than the C-ter pair (*32*).

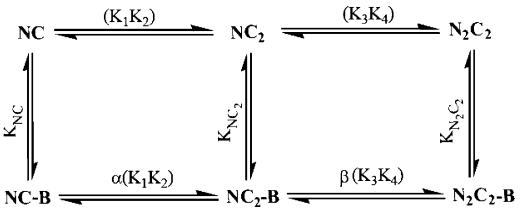


FIGURE 7: Minimal scheme for $Ca^{2+}$-dependent switching in the neuromodulin CaM−IQ domain complex. $Ca^{2+}$ binding via the N-ter → C-ter pathway depicted in the general scheme appears to be strongly disfavored, so it can be omitted from the minimal scheme describing the $Ca^{2+}$ dependence of the CaM−neuromodulin complex under steady-state conditions.

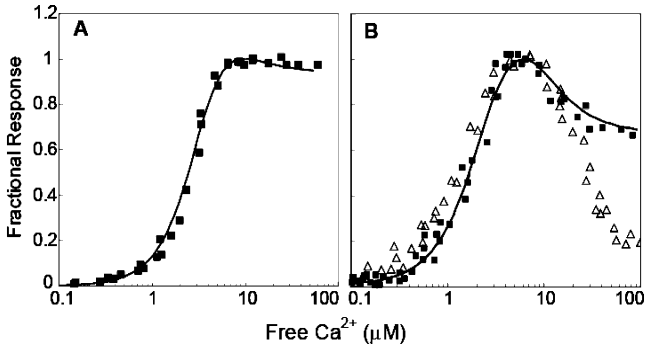


FIGURE 8: Bell-shaped relationship between the free $Ca^{2+}$ concentration and the dissociation constant for the complex between CaM and the neuromodulin IQ domain. All free $Ca^{2+}$ concentrations were verified using indo-5F or mag-indo-1. (A) Fractional fluorescence response of 250 nM BSCaM$_{IQ}$ in the presence of 20 $\mu$M CaM. (B) Fractional fluorescence response of 5 $\mu$M BSCaM$_{IQ}$ in the presence of 1 $\mu$M CaM (■) and fractional response of a solution of 1 $\mu$M ECFP−CaM and 5 $\mu$M EYFP−neuromodulin (△). Because the extent of FRET increases when this complex is formed, the fractional response in this case is defined as $(F - F_{min})/(F_{max} - F_{min})$. The curves in both panels were calculated as described in Materials and Methods according to the scheme depicted in Figure 7. The $F_{min}/F_{max}$ values used to generate these curves were adjusted slightly to achieve the fits shown. All adjusted values were within 3% of the mean values given in Table 1.

*Transition between the ApoCaM and $(Ca^{2+})_4$-CaM Complexes with BSCaM$_{IQ}$ and Full-Length Neuromodulin.* The results we have presented thus far are consistent with a minimal biphasic mechanism (Figure 7) in which the apparent affinity of the CaM−BSCaM$_{IQ}$ complex is decreased when $Ca^{2+}$ is bound to the C-ter EF hand pair in CaM and is restored to its initial value when $Ca^{2+}$ is bound to the N-ter EF hand pair. This mechanism should produce a bell-shaped relationship between the apparent dissociation constant for the CaM−BSCaM$_{IQ}$ complex and the free $Ca^{2+}$ concentration.

The fractional fluorescence response of 250 nM BSCaM$_{IQ}$ measured in the presence of 20 $\mu$M CaM is plotted versus the free $Ca^{2+}$ concentration in Figure 8A. The $EC_{50}(Ca^{2+})$ value for the transition between the apoCaM and $(Ca^{2+})_4$-CaM forms of the CaM−BSCaM$_{IQ}$ complex is 2.5 $\mu$M, and there appears to be little dissociation of the complex at any free $Ca^{2+}$ concentration. In contrast, the response of 5 $\mu$M BSCaM$_{IQ}$ measured in the presence of 1 $\mu$M CaM is bell-shaped, consistent with significant dissociation of the complex at intermediate free $Ca^{2+}$ concentrations. The

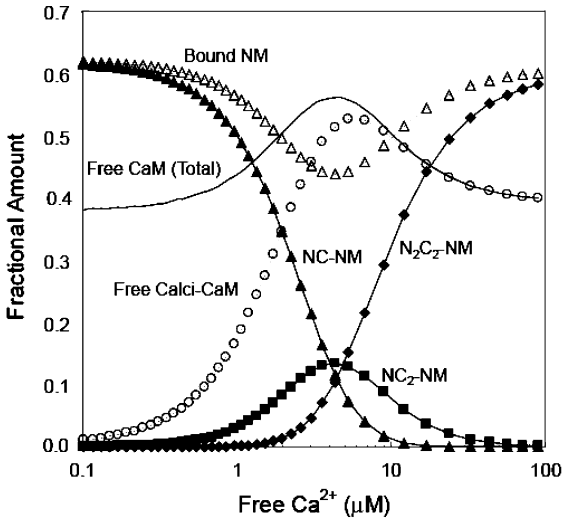


FIGURE 9: Various species produced in a solution of neuromodulin (NM) and CaM as a function of the free $Ca^{2+}$ concentration. Calculations were performed as described in Materials and Methods using CaM and NM concentrations of 10 $\mu$M on the basis of the scheme depicted in Figure 7. All calculated concentrations are expressed relative to the total CaM concentration. Curves correspond to the relative concentrations of bound NM (△), total free CaM (no symbol), free calci-CaM (○), the NCCaM−NM complex (▲), the $NC_2$CaM−NM complex (■), and the $N_2C_2$CaM−NM complex (◆). Calci-CaM refers to the total of all free $Ca^{2+}$-liganded CaM species, which primarily consist of $NC_2$CaM and $N_2C_2$−CaM. Otherwise, the nomenclature for the various $Ca^{2+}$-liganded species of CaM is given in the footnote of Table 1.

amount of dissociation appears to be maximal at a free $Ca^{2+}$ concentration of ~6 $\mu$M, and the rising and falling phases of this relationship have $EC_{50}(Ca^{2+})$ values of ~2 and ~11 $\mu$M, respectively. The agreement between the observed $BSCaM_{IQ}$ fluorescence responses and the theoretical curves calculated on the basis of our steady-state model is excellent under both sets of conditions (Figure 8A,B).

To verify the applicability of our results to the complex between CaM and full-length neuromodulin, we employed fluorescently labeled versions of CaM (ECFP−CaM) and full-length neuromodulin ($EYFP_C$−neuromodulin). As illustrated in Figure 1C, under 430 nm illumination, formation of the complex between these proteins results in an increase in fluorescence emission at 525 nm due to FRET between the CFP and $EYFP_C$ moieties. The fractional fluorescence response of a mixture of 5 $\mu$M $EYFP_C$−neuromodulin and 1 $\mu$M ECFP−CaM is plotted as a function of the free $Ca^{2+}$ concentration in Figure 8B. This relationship has a more marked bell shape than the accompanying $BSCaM_{IQ}$ response determined under essentially identical experimental conditions. This is because the complexes between labeled neuromodulin and labeled apoCaM or $(Ca^{2+})_4$-CaM have the same fluorescence emission, while the complexes between the two forms of CaM and $BSCaM_{IQ}$ have different emissions (Table 1 and Figure 1B). These results clearly demonstrate that the apparent dissociation constants for the complexes between CaM and $BSCaM_{IQ}$ or full-length neuromodulin have similar biphasic dependencies on the free $Ca^{2+}$ concentration.

## DISCUSSION

The relationship between the apparent dissociation constant for the complex between calmodulin (CaM) and the neuromodulin IQ domain and the free $Ca^{2+}$ concentration consists of two phases. In the first phase, $Ca^{2+}$ bound to the C-ter EF hand pair in CaM increases the $K_d$ for the complex from the $Ca^{2+}$-free value of 2.3 ± 0.1 $\mu$M to a value of 14.4 ± 1.3 $\mu$M. In the second phase, $Ca^{2+}$ bound to the N-ter EF hand pair reduces the $K_d$ for the complex to a value of 2.5 ± 0.1 $\mu$M, reversing the effect of the first phase. This behavior demonstrates that CaM−IQ domain complexes can function as a biphasic $Ca^{2+}$ switches through opposing effects of $Ca^{2+}$ bound sequentially to the two EF hand pairs in CaM. In the case of neuromodulin, these opposing effects serve to promote dissociation of CaM over a relatively narrow range of free $Ca^{2+}$ concentrations.

Gaertner and co-workers (*33*) recently published a study of the $Ca^{2+}$ dependencies of the CaM−neurogranin complex. This protein has essentially the same IQ domain as neuromodulin, and it is thought to have a similar CaM-buffering function (*34*). These investigators report that $Ca^{2+}$ is released from the CaM−neurogranin complex at an accelerated rate compared with the rate for free CaM, consistent with negative coupling, although they were unable to verify this with steady-state $Ca^{2+}$ binding measurements (*33*).

During a $Ca^{2+}$ signal in an excitable cell such as a neuron, CaM must be rapidly provided to targets such as CaM kinase II that have high local concentrations (*35*, *36*). It has been proposed that CaM-binding proteins such as neuromodulin provide the required local stores of CaM (*37*−*40*). However, if neuromodulin were simply to release CaM above a threshold free $Ca^{2+}$ concentration, any not taken up by targets would be free to diffuse away until the free $Ca^{2+}$ concentration fell below this threshold. Our results suggest that release of CaM from neuromodulin is promoted only within a relatively narrow 5−6-fold range in the free $Ca^{2+}$ concentration. Our current hypothesis is that during a $Ca^{2+}$ transient in a neuron the local free $Ca^{2+}$ concentration passes rapidly through this range, producing a transient burst of free CaM that rebinds neuromodulin if not taken up by targets. Maintenance of a defined distribution of CaM through this and similar mechanisms may be of particular importance in neurons and other cells whose specific responses to different types of $Ca^{2+}$ signals suggest a high degree of spatial discrimination (*41*−*43*).

The concentrations of the major species produced in a solution of CaM and neuromodulin as a function of the free $Ca^{2+}$ concentration can be calculated on the basis of the minimal mechanism presented in Figure 7 and the parameters listed in Tables 1 and 2. Given physiologically reasonable total neuromodulin and CaM concentrations of 10 $\mu$M, these calculations illustrate that essentially all of the CaM remains $Ca^{2+}$-free at $Ca^{2+}$ concentrations below 0.1 $\mu$M, with ~60% of the protein bound to the IQ domain. As the free $Ca^{2+}$ concentration is increased, the total concentration of free CaM increases by ~40% with an $EC_{50}(Ca^{2+})$ of ~2 $\mu$M, peaks at a free $Ca^{2+}$ concentration of ~5 $\mu$M, and declines back to the starting value with an $EC_{50}(Ca^{2+})$ of ~10 $\mu$M. To place the range of free $Ca^{2+}$ concentrations over which this occurs in a physiological context, it appears that local free $Ca^{2+}$ concentrations as high as 50−100 $\mu$M are produced in a variety of cell types, including neurons (*44*−*49*). There is of course also an inverse bell-shaped relationship between the concentration of the CaM−IQ domain protein complex and the free $Ca^{2+}$ concentration. This highlights the pos-

sibility that the switching mechanism we have identified produces biphasic responses in the activities of some IQ domain proteins.

## REFERENCES


1. Yagi, K., Yazawa, M., Kakiuchi, S., Ohshima, M., and Uenishi, K. (1978) Identification of an activator protein for myosin light chain kinase as the $Ca^{2+}$-dependent modulator protein, *J. Biol. Chem. 253*, 1338−1340.
2. Bredt, D. S., and Snyder, S. H. (1990) Isolation of nitric oxide synthetase, a calmodulin-requiring enzyme, *Proc. Natl. Acad. Sci. U.S.A. 87*, 682−685.
3. Venema, R. C., Sayegh, H. S., Arnal, J. F., and Harrison, D. G. (1995) Role of the enzyme calmodulin-binding domain in membrane association and phospholipid inhibition of endothelial nitric oxide synthase, *J. Biol. Chem. 270*, 14705−14711.
4. Dabrowska, R., Sherry, J. M., Aromatorio, D. K., and Hartshorne, D. J. (1978) Modulator protein as a component of the myosin light chain kinase from chicken gizzard, *Biochemistry 17*, 253−258.
5. Jurado, L. A., Chockalingam, P. S., and Jarrett, H. W. (1999) Apocalmodulin, *Physiol. Rev. 79*, 661−682.
6. Bahler, M., and Rhoads, A. (2002) Calmodulin signaling via the IQ motif, *FEBS Lett. 513*, 107−113.
7. Estep, R. P., Alexander, K. A., and Storm, D. R. (1990) Regulation of free calmodulin levels in neurons by neuromodulin: Relationship to neuronal growth and regeneration, *Curr. Top. Cell. Regul. 31*, 161−180.
8. Tran, Q. K., Black, D. J., and Persechini, A. (2003) Intracellular coupling via limiting calmodulin, *J. Biol. Chem. 278*, 24247−24250.
9. Rakhilin, S. V., Olson, P. A., Nishi, A., Starkova, N. N., Fienberg, A. A., Nairn, A. C., Surmeier, D. J., and Greengard, P. (2004) A network of control mediated by regulator of calcium/calmodulin-dependent signaling, *Science 306*, 698−701.
10. Isotani, E., Zhi, G., Lau, K. S., Huang, J., Mizuno, Y., Persechini, A., Geguchadze, R., Kamm, K. E., and Stull, J. T. (2004) Real-time evaluation of myosin light chain kinase activation in smooth muscle tissues from a transgenic calmodulin-biosensor mouse, *Proc. Natl. Acad. Sci. U.S.A. 101*, 6279−6284.
11. Tran, Q. K., Black, D. J., and Persechini, A. (2005) Dominant affectors in the calmodulin network shape the time courses of target responses in the cell, *Cell Calcium 37*, 541−553.
12. Gnegy, M. E. (1995) Calmodulin: Effects of cell stimuli and drugs on cellular activation, *Prog. Drug Res. 45*, 33−65.
13. Gerendasy, D. D., Herron, S. R., Watson, J. B., and Sutcliffe, J. G. (1994) Mutational and biophysical studies suggest RC3/neurogranin regulates calmodulin availability, *J. Biol. Chem. 269*, 22420−22426.
14. Persechini, A., and Cronk, B. (1999) The relationship between the free concentrations of $Ca^{2+}$ and $Ca^{2+}$-calmodulin in intact cells, *J. Biol. Chem. 274*, 6827−6830.
15. Persechini, A., and Stemmer, P. M. (2002) Calmodulin is a limiting factor in the cell, *Trends Cardiovasc. Med. 12*, 32−37.
16. Griesbeck, O., Baird, G. S., Campbell, R. E., Zacharias, D. A., and Tsien, R. Y. (2001) Reducing the environmental sensitivity of yellow fluorescent protein: Mechanism and applications, *J. Biol. Chem. 276*, 29188−29194.
17. Chapman, E. R., Au, D., Alexander, K. A., Nicolson, T. A., and Storm, D. R. (1991) Characterization of the calmodulin binding domain of neuromodulin. Functional significance of serine 41 and phenylalanine 42, *J. Biol. Chem. 266*, 207−213.
18. Persechini, A. (2002) Monitoring the intracellular free $Ca^{2+}$-calmodulin concentration with genetically-encoded fluorescent indicator proteins, *Methods Mol. Biol. 173*, 365−382.
19. Fruen, B. R., Black, D. J., Bloomquist, R. A., Bardy, J. M., Johnson, J. D., Louis, C. F., and Balog, E. M. (2003) Regulation of the RYR1 and RYR2 $Ca^{2+}$ release channel isoforms by $Ca^{2+}$-insensitive mutants of calmodulin, *Biochemistry 42*, 2740−2747.
20. Tang, W., Halling, D. B., Black, D. J., Pate, P., Zhang, J. Z., Pedersen, S., Altschuld, R. A., and Hamilton, S. L. (2003) Apocalmodulin and $Ca^{2+}$ calmodulin-binding sites on the $Ca_V1.2$ channel, *Biophys. J. 85*, 1538−1547.
21. Black, D. J., Tran, Q. K., and Persechini, A. (2004) Monitoring the total available calmodulin concentration in intact cells over the physiological range in free $Ca^{2+}$, *Cell Calcium 35*, 415−425.
22. Haiech, J., Klee, C. B., and Demaille, J. G. (1981) Effects of cations on affinity of calmodulin for calcium: Ordered binding of calcium ions allows the specific activation of calmodulin-stimulated enzymes, *Biochemistry 20*, 3890−3897.
23. Kilhoffer, M.-C., Kubina, M., Travers, F., and Haiech, J. (1992) Use of engineered proteins with internal tryptophan reporter groups and perturbation techniques to probe the mechanism of ligand-protein ineteractions: Investigation of the mechanism of calcium binding to calmodulin, *Biochemistry 31*, 8098−8106.
24. Evenas, J., Malmendal, A., Thulin, E., Carlstrom, G., and Forsen, S. (1998) $Ca^{2+}$ Binding and Conformational Changes in a Calmodulin Domain, *Biochemistry 37*, 13744−13754.
25. Malmendal, A., Evenas, J., Forsen, S., and Akke, M. (1999) Structural dynamics in the C-terminal domain of calmodulin at low calcium levels, *J. Mol. Biol. 293*, 883−899.
26. Linse, S., Johansson, C., Brodin, P., Grundström, T., Drakenberg, T., and Forsén, S. (1991) Electrostatic contributions to the binding of $Ca^{2+}$ in calbindin $D_{9k}$, *Biochemistry 30*, 154−162.
27. Linse, S., Helmersson, A., and Forsen, S. (1991) Calcium binding to calmodulin and its globular domains, *J. Biol. Chem. 266*, 8050−8054.
28. Andre, I., and Linse, S. (2002) Measurement of $Ca^{2+}$-binding constants of proteins and presentation of the CaLigator software, *Anal. Biochem. 305*, 195−205.
29. Alexander, K., Cimler, B., Meier, K., and Storm, D. (1987) Regulation of calmodulin binding to P-57. A neurospecific calmodulin binding protein, *J. Biol. Chem. 262*, 6108−6113.
30. Alexander, K., Wakim, B., Doyle, G., Walsh, K., and Storm, D. (1988) Identification and characterization of the calmodulin-binding domain of neuromodulin, a neurospecific calmodulin-binding protein, *J. Biol. Chem. 263*, 7544−7549.
31. Carlstrom, G., and Chazin, W. J. (1993) Two-dimensional $^1H$ nuclear magnetic resonance studies of the half-saturated ($Ca^{2+}$)1 state of calbindin D9k. Further implications for the molecular basis of cooperative $Ca^{2+}$ binding, *J. Mol. Biol. 231*, 415−430.
32. Forsén, S., Vogel, H. J., and Drakenberg, T. (1986) Biophysical studies of calmodulin, in *Calcium and Cell Function* (Cheung, W. Y., Ed.) pp 113−157, Academic Press, New York.
33. Gaertner, T. R., Putkey, J. A., and Waxham, M. N. (2004) RC3/neurogranin and $Ca^{2+}$/calmodulin-dependent protein kinase II produce opposing effects on the affinity of calmodulin for calcium, *J. Biol. Chem. 279*, 39374−39382.
34. Baudier, J., Deloulme, J. C., Van Dorsselaer, A., Black, D., and Matthes, H. W. (1991) Purification and characterization of a brain-specific protein kinase C substrate, neurogranin (p17). Identification of a consensus amino acid sequence between neurogranin and neuromodulin (GAP43) that corresponds to the protein kinase C phosphorylation site and the calmodulin-binding domain, *J. Biol. Chem. 266*, 229−237.
35. Strack, S., Choi, S., Lovinger, D. M., and Colbran, R. J. (1997) Translocation of Autophosphorylated Calcium/Calmodulin-Dependent Protein Kinase II to the Postsynaptic Density, *J. Biol. Chem. 272*, 13467−13470.
36. Colbran, R. J., and Soderling, T. R. (1990) Calcium/calmodulin-dependent protein kinase II, *Curr. Top. Cell. Regul. 31*, 181−221.
37. Prichard, L., Deloulme, J. C., and Storm, D. R. (1999) Interactions between Neurogranin and Calmodulin in Vivo, *J. Biol. Chem. 274*, 7689−7694.
38. Gamby, C., Waage, M. C., Allen, R. G., and Baizer, L. (1996) Growth-associated protein-43 (GAP-43) facilitates peptide hormone secretion in mouse anterior pituitary AtT-20 cells, *J. Biol. Chem. 271*, 10023−10028.
39. Gamby, C., Waage, M. C., Allen, R. G., and Baizer, L. (1996) Analysis of the Role of Calmodulin Binding and Sequestration in Neuromodulin (GAP-43) Function, *J. Biol. Chem. 271*, 26698−26705.
40. Gerendasy, D. D., and Sutcliffe, J. G. (1997) RC3/Neurogranin, A Postsynaptic Calpacitin For Setting The Response Threshold To Calcium Influxes, *Mol. Neurobiol. 15*, 131−163.
41. Hernandez-Cruz, A., Sala, F., and Adams, P. R. (1990) Subcellular calcium transients visualized by confocal microscopy in a voltage-clamped vertebrate neuron, *Science 247*, 858−862.
42. Deisseroth, K., Heist, E. K., and Tsien, R. W. (1998) Translocation of Calmodulin to the Nucleus Supports CREB Phosphorylation In Hippocampal Neurons, *Nature 392*, 198−202.
43. Bito, H., Deisseroth, K., and Tsien, R. W. (1996) CREB phosphorylation and dephosphorylation: A $Ca^{2+}$- and stimulus

duration-dependent switch for hippocampal gene expression, *Cell 87*, 1203−1214.
44. Etter, E. F., Minta, A., Poenie, M., and Fay, F. S. (1996) Near-membrane [$Ca^{2+}$] transients resolved using the $Ca^{2+}$ indicator FFP18, *Proc. Natl. Acad. Sci. U.S.A. 93*, 5368−5373.
45. Marsault, R., Murgia, M., Pozzan, T., and Rizzuto, R. (1997) Domains of high $Ca^{2+}$ beneath the plasma membrane of living A7r5 cells, *EMBO J. 16*, 1575−1581.
46. Davies, E. V., and Hallett, M. B. (1998) High micromolar $Ca^{2+}$ beneath the plasma membrane in stimulated neutrophils, *Biochem. Biophys. Res. Commun. 248*, 679−683.
47. Klingauf, J., and Neher, E. (1997) Modeling Buffered $Ca^{2+}$ Diffusion Near the Membrane: Implications for Secretion in Neuroendocrine Cells, *Biophys. J. 72*, 674−690.
48. Simon, S. M., and Llinas, R. R. (1985) Compartmentalization of the submembrane calcium activity during calcium influx and its significance in transmitter release, *Biophys. J. 48*, 485−498.
49. Llinas, R., and Moreno, H. (1998) Local $Ca^{2+}$ signaling in neurons, *Cell Calcium 24*, 359−366.

BI052533W